Melting Thresholds of Aluminum Irradiated by Ultraviolet Laser Pulses for Periodic Nanostructures Formation

Yongtao Jiang*1, Satoru Iwamori^{1,2}, and Masaki Hashida^{2,3}

¹Graduate School of Engineering, Course of Mechanical Engineering, Tokai University, 4-1-1 Kitakaname, Hiratsuka 252-1292, Japan

²RIST, Tokai University, 4-1-1 Kitakaname, Hiratsuka 252-1292, Japan

³ICR, Kyoto University, Gokasho, Uji 611-0011, Japan

*Corresponding author's e-mail: 4CEMM053@cc.u-tokai.ac.jp

For laser ablation of aluminum, ultraviolet Nd:YAG lasers were used with wavelengths of 355 nm and 266 nm (pulse durations of 5 ns and 6 ns, respectively, at repetition rate of 10 Hz). The melting threshold of aluminum was measured to be $F_{th,355} = 1.51$ J/cm² for 355 nm and $F_{th,266} = 0.76$ J/cm² for 266 nm. Periodic nanostructures were successfully produced on aluminum surfaces in the vicinity of laser-produced grooves. For the 355 nm laser, the structures formed at a fluence of 1.7 J/cm² to 2.2 J/cm² with the number of pulses N = 200 to 2000. The interspace of periodic nanostructures was 568 nm, as determined by 1D-fast Fourier transform on the average of 10 points. The depth of periodic nanostructures measured by atomic forced microscopy was 90 nm to 160 nm. For the 266 nm laser, the periodic nanostructures formed at a fluence of 1.0 J/cm² to 3.0 J/cm² with the number of pulses N = 300 to 500. The interspace of periodic nanostructures was 474 nm on average. The periodic nanostructures were oriented orthogonally to direction of laser polarization.

DOI: 10.2961/ilmn.2025.03.2007

Keywords: nanosecond pulsed laser, aluminum, melting threshold, periodic nanostructures, ultraviolet laser

1. Introduction

Aluminum, known for its light weight, high strength, and good electrical and thermal conductivity, is widely used in various industrial fields, including aerospace, automotive, and electronics. However, conventional mechanical processing methods involve significant challenges in accurately forming complex micro-nanostructures on aluminum surfaces, limiting their potential in advanced manufacturing and functional surface engineering. Ultraviolet (UV) nanosecond lasers are increasingly gaining attention for their applications in material processing and surface modification, particularly in forming micro-nanostructures on metal surfaces.

One of the key advancements in this field is the laser-induced periodic surface structuring (LIPSS). The LIPSS technique is notable for its ability to produce highly controllable and repeatable periodic micro-nanostructures [1]. These structures can significantly enhance the surface properties of materials, providing aluminum surfaces with increased hardness, wear resistance, and corrosion resistance [2]. Additionally, LIPSS can impart unique optical, electrical, and biocompatibility properties [3] [4] that are difficult to achieve with conventional processing methods. The high energy density and short pulse duration of UV lasers make them particularly well suited to forming LIPSS [5], allowing for excellent precision and control at the nanoscale.

A promising application of LIPSS on aluminum (anode collector) is improving the performance of lithium-ion batteries. By increasing the surface area of the anode collector $(V_2O_3/C \text{ composite})$, the capacity and overall performance of the batteries can be significantly enhanced [6]. However, due to aluminum's high reflectivity and thermal conductivity,

creating clear periodic nanostructures on its surface is particularly challenging [7]. Although femtosecond lasers are commonly used to create LIPSS, achieving large-area LIPSS formation on aluminum remains difficult, and their high cost and complexity limit practical applications [8]. Therefore, this study explores the use of 355 nm and 266 nm UV Nd:YAG lasers for LIPSS formation. We found that appropriate laser irradiation conditions successfully generated periodic nanostructures on the aluminum surface irradiated with 355 nm or 266 nm UV Nd:YAG laser pulses. Additionally, microstructures on collector can further improve the performance of lithium-ion batteries.[9]

In this paper, the formation of microstructures and periodic nanostructures on aluminum with 355 nm and 266 nm UV Nd:YAG lasers is reported.

2. Experimental

For measurement of the melting threshold and formation of the surface structuring, ultraviolet laser pulses generated from Nd:YAG laser systems were utilized. The wavelength of 355 nm was derived from a Power Lite PL8000 system (Lumibird, Co. Ltd.) with a pulse duration of 5 ns, a beam diameter of 7.35 mm, and linear polarization in the horizontal direction. The wavelength of 266 nm was generated from a Sure lite III-10 (Lumibird, Co. Ltd.) with a pulse duration of 6 ns and a beam diameter of 7.45 mm. The laser pulse was focused onto the aluminum surface through a convex lens with a focal length of f=200 mm to a spot size of 35 μ m \pm 1 μ m at full width at e⁻¹ intensity maximum (FWe⁻¹M) for the 355 nm laser, and 40 μ m \pm 1 μ m for the 266 nm laser. The laser had a Gaussian spatial distribution on aluminum

surface as measured with a CMOS camera. The laser pulse energy was measured with a pyroelectric detector (PE9C, Ophir Optronics Solutions) and was adjusted from 9.4 μ J to 268 μ J using a half-wave plate and a polarizing prism (energy attenuator). The laser fluence, defined as the irradiated laser energy per unit area, was controlled from 0.76 J/cm² to 20 J/cm².

The aluminum was mounted on a motorized X-Y stage, and the scanning speed was adjusted so that the number of irradiated laser pulses was N = 5, 10, or 20.

The aluminum (AL-013558, 99.999%, The Nilaco Corp.) had dimensions of 15 mm \times 15 mm with a thickness of 2 mm, and its surface was mechanically polished to an arithmetic mean surface roughness of less than Ra < 0.8 nm on the untreated aluminum.

The surface morphology of aluminum irradiated with laser pulses was measured by using a laser scanning microscope equipped with atomic forced microscopy (LEXT4500, Olympus), a desktop scanning electron microscope (SEM; TM4000PlusII, Hitachi High-Technologies), and a field emission SEM (FE-SEMJSM-7800F, JEOL Ltd.). The elemental composition of the aluminum surface was measured by X-ray photoelectron spectroscopy (XPS; PHIQuanterall, Ulvac-PHI).

3. Results and discussion

3.1 Melting threshold measurement and calculation

Fig. 1(a) shows a laser-produced crater on the aluminum surface at a laser fluence $F = 5.0 \text{ J/cm}^2$ for N = 10 pulses. Fig. 1(b) shows a cross-sectional view of the crater profile in the vertical direction. The crater diameter, defined as the distance from the rising edge of the upper side to that of the lower side, was measured to be 59.7 µm. The craters on the aluminum surface were produced in the laser fluence range from 0.76 J/cm² to 20 J/cm² as measured with a scanning laser microscope. The diameters of craters were analyzed as a function of laser fluence [10] [11] and are plotted in Fig. 2 as solid circles. The experimental data were fit well with a Gaussian distribution at the irradiated spot on the aluminum surface. Extrapolation of the curve showed a melting threshold of $F_{\text{th,355}} = 1.51 \text{ J/cm}^2$ for the 355 nm laser and $F_{\text{th,266}} =$ 0.76 J/cm² for the 266 nm laser. The experimental results show that as the laser wavelength becomes longer, the melting threshold of aluminum increases. For the formation of grooves and periodic nanostructures, we used the laser fluence about 1.5 times higher than $F_{th, 355}$ and 2.0 times higher

Experimentally observed melting thresholds of aluminum were compared with those calculated using a one-dimensional thermal diffusion model proposed by Sparks [12]. The theoretical calculation for the melting threshold fluence (F_{th}) is given by:

$$F_{th} = \frac{(T_m - T_0)\sqrt{\pi C_i k_i}}{2A} \sqrt{\tau_L}, \qquad (1)$$
 where T_m is the melting temperature, T_0 is the room temper-

where T_m is the melting temperature, T_0 is the room temperature, C_i is the heat capacity, K_i is the thermal conductivity, A is the laser pulse absorption, and τ_L is the pulse duration. The aluminum properties are summarized in Table 1. Using these parameters, the calculated melting threshold of aluminum was 1.19 J/cm² for the 355 nm laser and 1.39 J/cm² for the 266 nm laser.

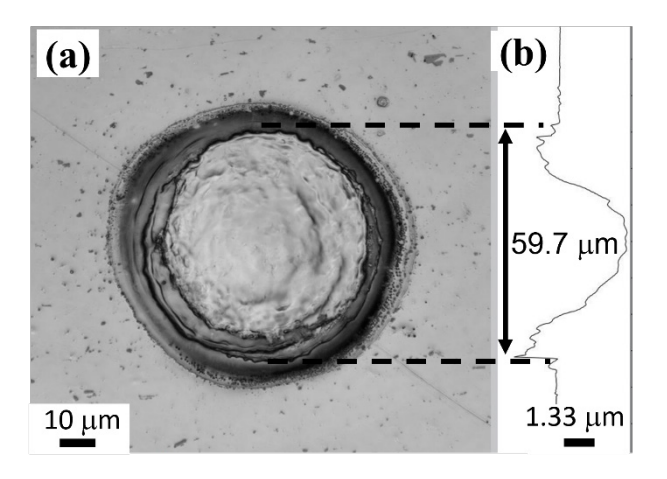


Fig. 1 Laser-produced crater on the aluminum surface ($F = 5.0 \text{ J/cm}^2$, N = 10 pulses).

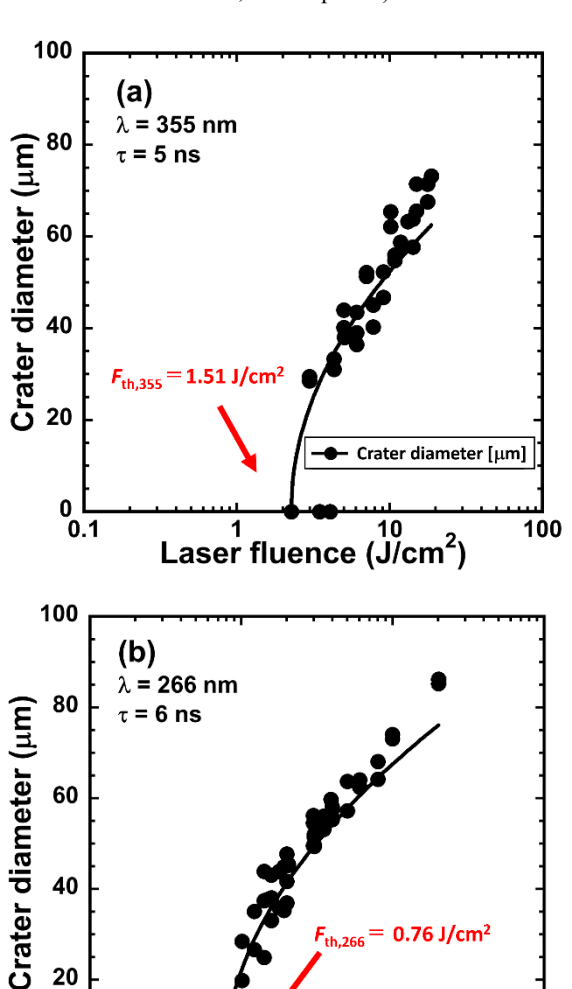


Fig. 2 Crater dependence on laser fluence.

Laser fluence (J/cm²)

0.1

Crater diameter [µm]

100

10

Table 1 Material properties of aluminum for melting threshold	
calculation.	

Property	Notation	Value
Melting temperature	$T_{ m m}$	933.5 K
Room temperature	T_0	297.15K
Heat capacity	$C_{\rm i}$	2.43 J/cm ³ /K
Thermal conductivity	k_{i}	2.37 W/cm/K
Absorption	A_{355}	0.08 [9]
	A_{266}	0.07527 [10]

The discrepancy between the experimental and theoretical values might be attributable to low laser absorption (higher reflection) at the laser spot. For such higher reflection, the melting threshold of aluminum might be sensitive to surface roughness for shorter laser wavelengths.

3.2 Surface structuring experiment

For surface structuring on the aluminum surface, the laser pulse was focused through a cylindrical lens with a focal length of 300 mm to a spot size of 27 μ m (vertical) \times 7.35 mm (horizontal) for the 355 nm laser, and 14 µm (vertical) × 7.45 mm (horizontal) for the 266 nm laser. The laser pulse energy was adjusted from 0.9 mJ to 8.2 mJ using a half-wave plate and a polarizing prism. A pyroelectric detector (PE25C, Ophir Optronics Solutions) was employed to measure the laser pulse energy. The laser fluence was controlled from 0.8 J/cm² to 4.2 J/cm². The irradiated spot with the cylindrical lens was also measured using the CMOS camera. At the laser spot, the spatial distribution was a Gaussian distribution in the vertical direction and a top hat distribution in the horizontal direction. The aluminum was mounted on a motorized X-Y stage, and the scanning speed was adjusted so that the number of irradiated pulses ranged from N = 50 to 4000. To fabricate the groove on the surface, the aluminum was scanned in the horizontal direction. The laser polarization direction was parallel to the scanning direction. To fabricate the lattice structure, the horizontal grooves were first formed at a hatching distance of 160 µm, and then the sample was rotated 90° to create vertical grooves, thereby forming the lattice structure.

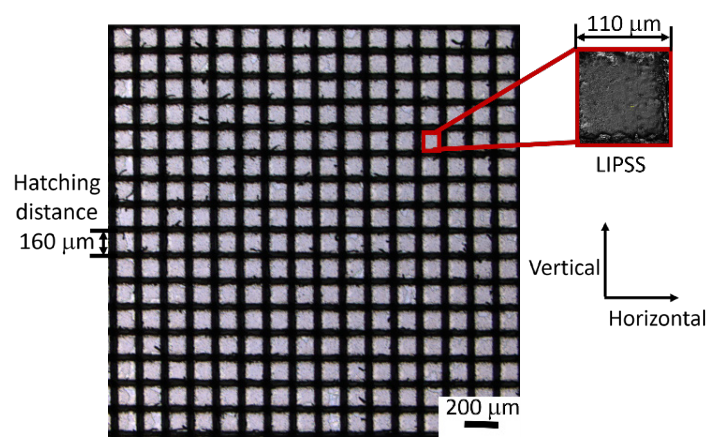


Fig. 3 Micro-groove structure formed with a 355 nm laser at a laser fluence of $1.5F_{th,355}$ for N = 500 pulses.

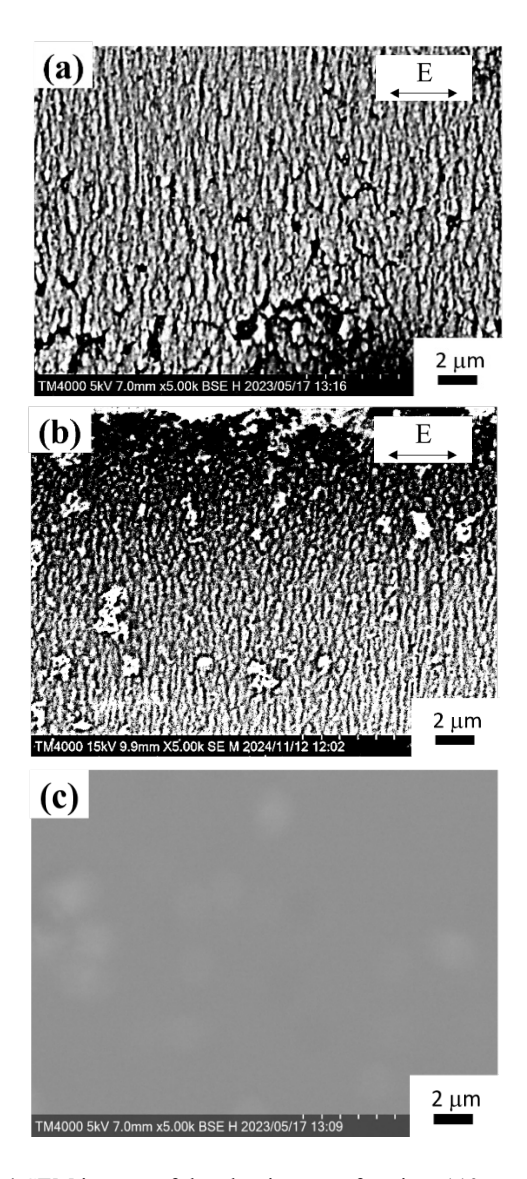


Fig. 4 SEM images of the aluminum surface in a 110 μ m \times 110 μ m with the 266 nm laser. (c) Surface of pristine aluminum. The arrows labeled E show the laser polarization direction.

Fig. 3 shows the lattice structure, which consists of micro-groove structure (black) with a hatching distance of 160 μm in the vertical and horizontal directions. With the 355 nm laser, the groove was produced at a laser fluence of $1.5F_{\text{th},355}$ for N=500 pulses. The groove is 50 $\mu m\pm 2~\mu m$ wide and 20 $\mu m\pm 2~\mu m$ deep. With the 266 nm laser, the groove was 52 $\mu m\pm 2~\mu m$ wide and 21 $\mu m\pm 2~\mu m$ deep, which are comparable to the results obtained with the 355 nm laser. The 110 $\mu m\times 110~\mu m$ area located outside of grooves showed uniform formation of periodic nanostructures.

Fig. 4(a) and (b) are FE-SEM images near the grooves. Although the 110 μ m \times 110 μ m area in Fig. 3 seems to be a smooth surface, periodic nanostructures were formed uniformly as shown in Fig. 4(a) and (b); for comparison, Fig. 4(c) shows the pristine surface of aluminum.

3.3 Formation of periodic structures

Fig. 4(a) shows periodic nanostructures formed with 355 nm pulses at a laser fluence of $1.5F_{\rm th,355}$ for N=500 pulses. With the 355 nm laser, the structures formed at fluence ranging from $1.13F_{\rm th,355}$ (= 1.7 J/cm²) to $1.5F_{\rm th,355}$ (= 1.7 J/cm²) for $1.5F_{\rm th,355}$ (= 1.5 J/cm²) for $1.5F_{\rm th,266}$ for $1.5F_{\rm th,266}$ for $1.5F_{\rm th,266}$ (= $1.5F_{\rm th,266}$ (= 1.

3.4 FFT analysis of LIPSS periodicity

To analyze the periodicity of the nanostructures, 1D-fast Fourier transform (1D-FFT) [15] was applied to SEM images. FFT spectrum on the average of 10 points is shown in Fig. 5(a) for 355 nm and in Fig. 5 (b) for 266 nm. The results show that the periodicity Λ of the structure was about 568 nm for the 355 nm laser and about 474 nm for the 266 nm. Though the periodicity Λ is a few times larger than the laser wavelength, it might be related to the laser wavelength.

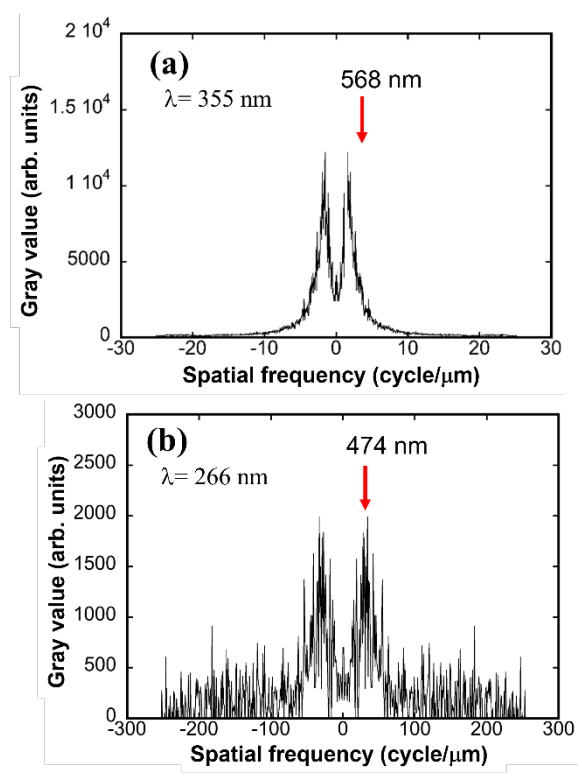


Fig. 5 One-dimensional FFT spectra (a) at $1.5F_{\text{th},355}$ for N = 500 pulses with the 355 nm laser and (b) at $2.0F_{\text{th},266}$ for N = 300 pulses with the 266 nm laser.

3.5 Measurement of surface area of lattice structure and nanostructures

The surface area was measured with a laser scanning microscope for the lattice structure and with an atomic forced microscopy for the nanostructures. The increase in surface area with laser irradiation was 4.6 times for the lattice structure and 2.2 times for the nanostructures. The total increase of surface area was 6.8-fold. To estimate the surface area after laser irradiation, the experimentally observed structures characterized to have a width/depth ratio of 3.5 were

used. These were shown to have a 1.49-fold increase in surface area for lattice structures and a 2.07-fold increase in surface area for nanostructures, for a total of 3.56-fold. The reason for the difference between the experimental and calculated values might be the higher roughness of the grooves.

3.6 Elemental composition

XPS was used to investigate the chemical changes on the aluminum surface. The pristine aluminum surface and the laser-induced nanostructure (LIPSS region) and lattice structure inside the groove were analyzed. Table 2 presents the results for aluminum [16]-[18] and oxygen [19][20] content, showing an increase in oxygen after laser processing. This suggests that the laser processing caused an oxidation reaction on the aluminum surface.

Table 2 Surface chemical changes on aluminum.

Ele-	Al	Al with	Pristine Al
ment	groove,	LIPSS, 355	
	355 nm	nm	
Al	16.2%	11.4%	35.9%
О	83.8%	88.6%	64.1%

3.7 Discussion

To discuss why periodic structures were produced in the vicinity of grooves, we considered a previous report [21] that estimated the propagation of a surface plasma wave (SPW) as shown in Fig. 6. When a laser pulse is irradiated on aluminum above the threshold fluence, the surface is heated above the melting temperature. At the same time, the laser pulse might induce a SPW [22][23] that propagates to the outer side as shown in Fig. 6. The propagation area of the SPW was irradiated with low laser fluence since the laser beam has a Gaussian spatial distribution. The propagating SPW might interact with low laser fluence components and produce periodic nanostructures. The SPW propagation length $L_{\rm SPP}$ was calculated using the following equation [21]:

$$L_{\rm spp} = \frac{1}{2\,(\beta)} \ , \tag{2}$$

$$\beta = \pm \frac{\omega}{c} \sqrt{\frac{\varepsilon_{air} \varepsilon_{Al_355}}{\varepsilon_{air} + \varepsilon_{Al_355}}} , \qquad (3)$$

$$\frac{\omega}{c} = \frac{2\pi}{\lambda} \ . \tag{4}$$

Here, ω is the laser frequency, c is the speed of light, ε is the permittivity of air or aluminum, and λ is the laser wavelength. Table 3 summarizes the permittivity for calculating the propagation length in equation (2).

The propagation length was $7.23\,\mu m$ for $355\,nm$ and only $0.74\,\mu m$ for $266\,nm$. The nanostructures formed with the $355\,nm$ laser had higher uniformity than those formed with the $355\,nm$ laser as shown by the FFT spectrum and

Table 3 Permittivity of materials.

Material	Notation	Permittivity	Ref.
Air	\mathcal{E}_{air}	1	
Aluminum for 355nm	\mathcal{E}_{Al_355}	-50.36+23.56i	[25]
Aluminum for 266nm	\mathcal{E}_{Al_266}	-8.66+12.36i	[25]

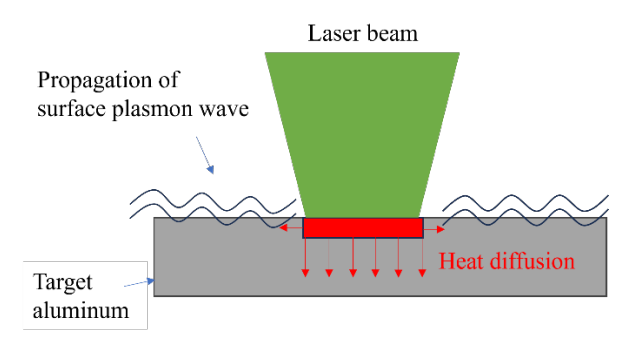


Fig. 6 Propagation of an SPW induced by a laser pulse.

SEM images, because the propagation length for 355 nm was 10-fold that for 266 nm. Further investigation is needed to determine why the period of nanostructures was wider than the laser wavelength.

4. Conclusions

The melting threshold of aluminum was measured experimentally with the crater diameter dependence on laser fluence for 355 nm and 266 nm UV lasers. The melting threshold was $F_{\rm th,355}=1.51~\rm J/cm^2$ for 355 nm and $F_{\rm th,266}=0.76~\rm J/cm^2$ for 266 nm. A lattice structure consisting of micro-grooves with a hatching distance of 160 µm in the vertical and horizontal directions was produced. The grooves were produced at a laser fluence of $1.5F_{\rm th,355}$ for $N=500~\rm pulses$ with the 355 nm laser. The periodic nanostructures were produced in a 110 µm \times 110 µm area in the vicinity of grooves. The periodicity of the structure was about 568 nm for the 355 nm laser and about 474 nm for the 266 nm laser. We found that the surface area increased 6.8-fold compared with the pristine surface when the lattice structure and nanostructures formed on the aluminum surface.

For formation mechanism of periodic nanostructures, the propagation of an SPW was considered. The propagating SPW might interact with low-fluence components of the laser to produce the periodic nanostructures.

The increased surface area and hierarchical micro/nanostructures are expected to enhance the performance of lithium-ion batteries by improving the adhesion between active materials and the current collector, facilitating electrolyte wetting, and reducing interfacial resistance. Offermann et al. reported [25] that surface-structured aluminum current collectors significantly improved mechanical interlocking and battery performance compared with flat surfaces. Although electrochemical performance measurements were not conducted in this study, the fabricated structures are anticipated to provide similar benefits, and future work will evaluate their impact on actual battery performance.

Acknowledgements

This research was financially supported by Grants-in-Aid for Scientific Research (C) (JP16K06745, 22K04766, 24K08287) from the Ministry of Education, Culture, Sports, Science and Technology (MEXT), Japan; the New Energy Industrial Technology Development Organization (NEDO) /Ministry of Economy, Trade and Industry, Japan; MEXT Quantum Leap Flagship Program (MEXT Q-LEAP) Grant Number JPMXS0118070187; the AMADA Foundation (AF-2022233-B3); and the Advanced Analysis Centre in

Research Institute of Science and Technology of Tokai University.

References

- [1] J. Bonse and B. Korte: Appl. Surf. Sci., 356, (2015) 203.
- [2] J. Outon, T. Cordoba, E. Gallero, M. Vlahou, E. Stratakis, V. Matres, and E. Blanco: J. Mater. Res. Technol., 27, (2023) 7422.
- [3] J. Bonse, S. Höhm, S. V. Kirner, A. Rosenfeld, and J. Krüger: IEEE J. Sel. Top. Quantum Electron., 23, (2017) 7422.
- [4] M. Okazaki, M. Hashida, and S. Iwamori: J. Laser Appl., 35, (2024) 042075.
- [5] S. E. Clark and D. C. Emmony: Phys. Rev. B, 40, (1989) 2031.
- [6] K. Ji-Hwan, K. Yo-Seob, M. Sang-Hyun, P. Deok-Hye, K. Min-Cheol, C. Jin-Hyeok, S. Jae-Hoon, and P. Kyung-Won: Electrochim. Acta, 389, (2021) 138685.
- [7] Z. Ou, M. Huang, and F. Zhao: Opt. Laser Technol., 79, (2016) 79.
- [8] L. Evgeny, L. Yoann, and M. Nadezhda: Nanomaterials, 10, (2020) 1836.
- [9] W. Pfleging and P. Gotcu: Appl. Sci., 9, (2019) 3588.
- [10] J. Jamdeleit, G. Urbasch, H. D. Hoffmann, H.-G. Treush, and E. W. Kreutz: Appl. Phys. A, 63, (1996) 117.
- [11] M. Hashida, A. F. Semerok, O. Gobert, G. Petit, Y. Izawa, and J. F. Wagner: Appl. Surf. Sci., 197-198, (2002) 862.
- [12] M. Sparks and E. Loh, Jr.: J. Opt. Soc. Am., 69, (1979) 847.
- [13] F. Cheng, P.-H. Su, J. Choi, S. Gwo, X. Li, and C.-K. Shih: ACS Nano, 10, (2016) 9852.
- [14] K. M. McPeak, S. V. Jayanti, S. J. P. Kress, S. Meyer, S. Iotti, A. Rossinelli, and D. J. Norris: ACS Photon., 2, (2015) 326.
- [15] K. Takenaka, M. Hashida, H. Sakagami, S.-i. Masuno, M. Kusaba, S. Yamaguchi, S. Iwamori, Y. Sato, and M. Tsukamoto: Rev. Sci. Instrum., 93, (2022) 093001.
- [16] V. I. Nefedov: J. Electron Spectrosc. Relat. Phenom., 25, (1982) 29.
- [17] G. E. McGuire, G. K. K. Schweitzer, and T. A. Carlson: Inorg. Chem., 12, (1973) 2451.
- [18] V. I. Nefedov, Y. V. Salyn, G. Leonhardt, and R. Scheibe: J. Electron Spectrosc. Relat. Phenom., 10, (1977) 121.
- [19] T. L. Barr: Appl. Surf. Sci., 15, (1983) 1.
- [20] C. D. Wagner, D. E. Passoja, H. F. Hillery, G. T. Six, H. A. Jansen, and J. A. Taylor: J. Vac. Sci. Technol., 21, (1982) 933.
- [21] I. Gnilitskyi, T. J.-Y. Derrien, Y. Levy, N. M. Bulgakova, T. Mocek, and L. Orazi: Sci. Rep., 7, (2017) 8485.
- [22] S. Sakabe, M. Hashida, S. Tokita, S. Namba, and K. Okamuro: Phys. Rev. B, 79, (2009) 033409.
- [23] M. Hashida, Y. Ikuta, Y. Miyasaka, S. Tokita, and S. Sakabe: Appl. Phys. Lett., 102, (2013) 174106.
- [24] A. D. Rakić, A. B. Djurišić, J. M. Elazar, and M. L. Majewski: Appl. Opt., 37, (1998) 5271.
- [25] J. Offermann, E. Gayretli, C. Schmidt, J. Carstensen,

H.-G. Bremes, A. Würsig, S. Hansen, M. Abdollahifar, and R. Adelung: J. Colloid Interface Sci., 664, (2024) 444.

(Received: June 24, 2025, Accepted: October 10, 2025)